Influence of apical oxygen on the extent of in-plane exchange interaction in cuprate superconductors

Y. Y. Peng[1], G. Dellea[1], M. Minola[2], M. Conni[1], A. Amorese[3], D. Di Castro[4], G. M. De Luca[5,6], K. Kummer[3], M. Salluzzo[6], X. Sun[7], X. J. Zhou[7], G. Balestrino[4], M. Le Tacon[2,8], B. Keimer[2], L. Braicovich[1,9], N. B. Brookes[3] and G. Ghiringhelli[1,9]*

In high-T_c superconductors the magnetic and electronic properties are determined by the probability that valence electrons jump virtually from site to site in the CuO_2 planes, a mechanism opposed by on-site Coulomb repulsion and favoured by hopping integrals. The spatial extent of the latter is related to transport properties, including superconductivity, and to the dispersion relation of spin excitations (magnons). Here, for three antiferromagnetic parent compounds (single-layer $Bi_2Sr_{0.9}La_{1.1}CuO_{6+\delta}$, double-layer $Nd_{1.2}Ba_{1.8}Cu_3O_6$ and infinite-layer $CaCuO_2$) differing by the number of apical atoms, we compare the magnetic spectra measured by resonant inelastic X-ray scattering over a significant portion of the reciprocal space and with unprecedented accuracy. We observe that the absence of apical oxygens increases the in-plane hopping range and, in $CaCuO_2$, it leads to a genuine three-dimensional (3D) exchange-bond network. These results establish a corresponding relation between the exchange interactions and the crystal structure, and provide fresh insight into the materials dependence of the superconducting transition temperature.

In copper-based high-critical-temperature (high-T_c) superconductors the detailed electronic structure close to Fermi level and the short- and mid-range magnetic interactions are governed by the same physical parameters, namely the interatomic hopping integrals and the on-site Coulomb repulsion[1]. Therefore, superconductivity, magnetism and charge density modulations are intimately related in cuprates, and any model for transport properties has to comply with the two other properties. Conversely, the determination of hopping parameters from magnetic measurements can help clarify the origin of superconductivity. The energy scale of spin excitations at the magnetic Brillouin zone boundary (250–400 meV) is mainly determined by the large nearest-neighbour Cu–Cu superexchange interaction (J), and makes spin fluctuations a good candidate for Cooper pairing in high-T_c superconductors[2]. This common property is easily traced back to the two-dimensional CuO_2 square lattice of all layered cuprates, where the Cu–O–Cu double bond has very similar length (3.8–3.9 Å) and angle (174°–180°) in all families, irrespective of the different out-of-plane structure. Attempts at correlating the value of J with the critical temperature at optimal doping ($T_{c,max}$) did not reach consensus[3–5] because disorder, buckling and other properties can be more relevant than bare superexchange[6]. Indeed such large J preserves short range in-plane antiferromagnetic correlation up to room temperature in undoped compounds, and well above optimal doping level in superconductors: the sharp and dispersing magnetic excitations measured by inelastic neutron scattering (INS)[7,8] or resonant inelastic X-ray scattering (RIXS)[9–12] in

insulating compounds, survive in a damped, broadened form (paramagnon) throughout the superconducting phase diagram[9,13–15].

However, longer-range electronic (and spin) correlations are those that determine the exact shape of the spin excitation dispersion, which is peculiar to each family of cuprates. It was shown by Coldea *et al.*[7] that in La_2CuO_4 (LCO) the magnon dispersion can be adequately reproduced by considering a cyclic exchange beyond the nearest-neighbour Heisenberg term. It is common to tie down those longer-range effective exchange integrals by expressing them in terms of Hubbard model parameters—that is, the nearest-neighbour (Cu to Cu) hopping integral t and the Coulomb repulsion U, where next-nearest-neighbour hopping, described by multiple jumps, is proportional to higher powers of t. This approximation can reproduce a sizable energy dispersion along the magnetic Brillouin zone boundary (MBZB), but it usually leads to unphysically small U, and cannot fully account for the departure from a sine law of the energy dispersion $E(\mathbf{q}_\parallel)$ along the (1,0) direction[7,11,16]. The bare inclusion, in the one-band Hubbard model, of next-nearest-neighbour hopping parameters t' and t'' further improves the fitting to experimental results for La_2CuO_4, $Sr_2CuO_2Cl_2$ and Y-doped Bi2212 (ref. 17), but cannot be easily related to the other properties of those materials. Pavarini *et al.*[18], by considering a Hubbard model including Cu4s, Cu3d_{z^2} and apical-O2p_z (in addition to the usual in-plane Cu3$d_{x^2-y^2}$ and O2$p_{x,y}$), suggested larger intralayer hopping range leads to higher $T_{c,max}$.

[1]Dipartimento di Fisica, Politecnico di Milano, Piazza Leonardo da Vinci 32, I-20133 Milano, Italy. [2]Max-Planck-Institut für Festkörperforschung, Heisenbergstraße 1, D-70569 Stuttgart, Germany. [3]ESRF, The European Synchrotron, 71 Avenue des Martyrs, F-38043 Grenoble, France. [4]CNR-SPN and Dipartimento di Ingegneria Civile e Ingegneria Informatica, Università di Roma Tor Vergata, Via del Politecnico 1, I-00133 Roma, Italy. [5]Dipartimento di Fisica"E. Pancini", Università di Napoli Federico II, Complesso Monte Sant'Angelo, Via Cinthia, I-80126 Napoli, Italy. [6]CNR-SPIN, Complesso MonteSantangelo - Via Cinthia, I-80126 Napoli, Italy. [7]Beijing National Laboratory for Condensed Matter Physics, Institute of Physics, Chinese Academy of Sciences, Beijing 100190, China. [8]Institute of Solid State Physics (IFP), Karlsruhe Institute of Technology, D-76021 Karlsruhe, Germany. [9]CNR-SPIN, Dipartimento di Fisica, Politecnico di Milano, Piazza Leonardo da Vinci 32, I-20133 Milano, Italy. *e-mail: giacomo.ghiringhelli@polimi.it
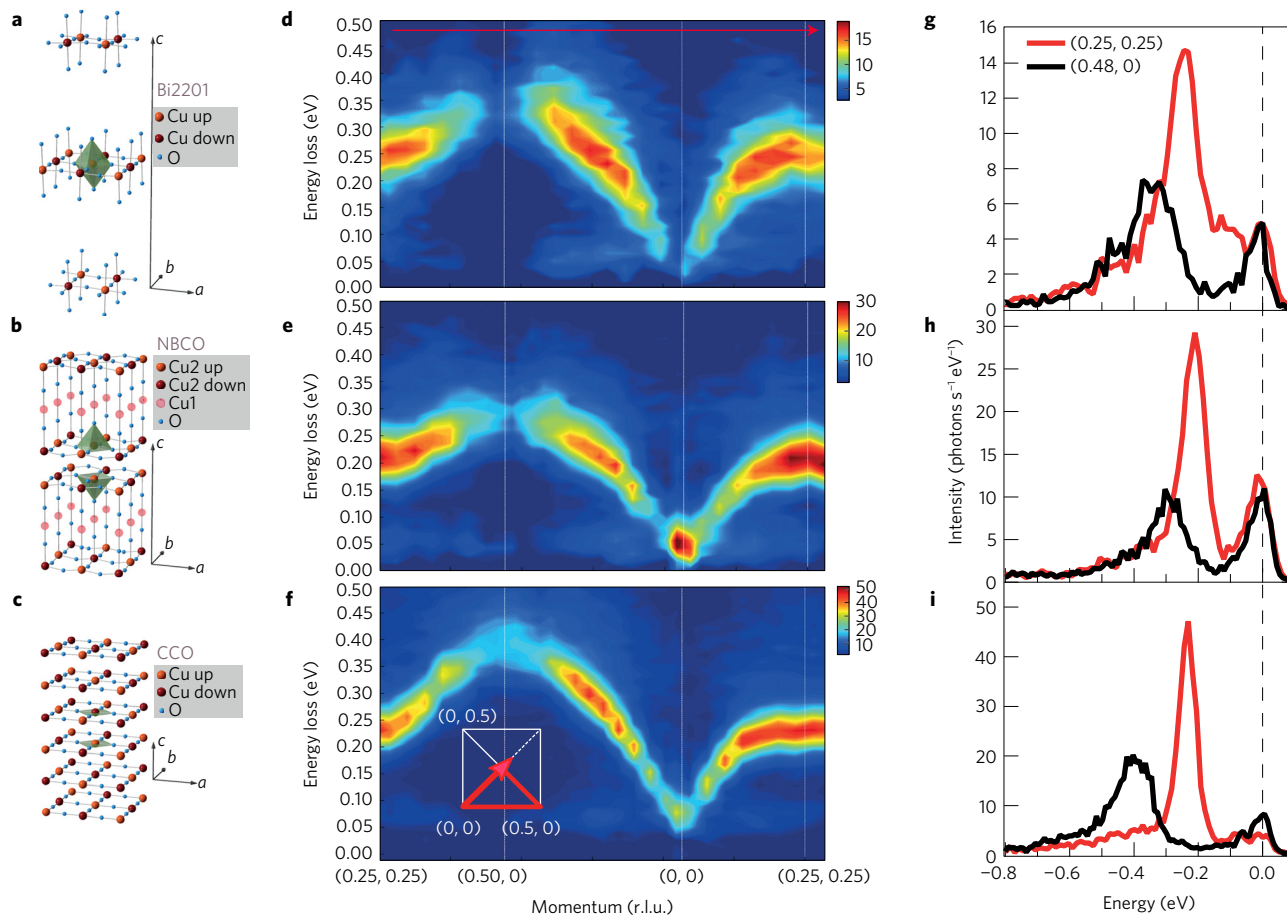
Figure 1 | In-plane momentum dependence of the magnetic excitations of antiferromagnetic layered cuprates measured by RIXS at the Cu L_3 resonance.
a–c, Partial crystalline structures of $Bi_2Sr_{2-x}La_xCuO_6$, $NdBa_2Cu_3O_{6+x}$ and $CaCuO_2$. **d–f**, Spin-wave dispersion of heavily underdoped $Bi_2Sr_{2-x}La_xCuO_6$ ($p = 0.03$), undoped $NdBa_2Cu_3O_{6+x}$, and $CaCuO_2$, respectively, along the high-symmetry momentum trajectory indicated in the inset of **f**. Elastic peaks were subtracted for a better visualization of the low-energy features. **g–i**, Raw spectra for Bi2201, NBCO and CCO, respectively, at high-symmetry points $\mathbf{q}_\parallel = (0.25, 0.25)$ (red) and $\mathbf{q}_\parallel = (0.48, 0)$ (black) belonging to the antiferromagnetic Brillouin zone boundary: the comparison highlights the differences in intensity, energy and width between the two points, and the actual elastic contribution.

Here, by exploiting the new experimental capabilities of Cu L_3 edge RIXS, we determine the magnon dispersion of three antiferromagnetic (AF) cuprates over the whole magnetic Brillouin zone, analyse the results within the Heisenberg model with extended exchange terms, and relate them to the crystalline structure. Figure 1 provides a comprehensive overview of our experimental results for three materials differing by the number of apical oxygens per Cu atom: single-layer $Bi_2Sr_{0.9}La_{1.1}CuO_{6+\delta}$ (Bi2201, $p = 0.03$) (ref. 19), bilayer $Nd_{1.2}Ba_{1.8}Cu_3O_6$ (NBCO) (ref. 20) and infinite-layer $CaCuO_2$ (CCO) (ref. 21). RIXS spectra were measured at equally spaced points in the in-plane reciprocal space, along the $(1/4, 1/4) \rightarrow (1/2, 0) \rightarrow (0, 0) \rightarrow (0.3, 0.3)$ path (Fig. 1f, inset), fully representative of the first magnetic Brillouin zone. The out-of-plane momentum $L \neq 0$ changes along the path and differs from sample to sample. Bi2201 is constituted by two CuO_2 planes per unit cell with a $(1/2, 1/2)$ stacking offset, each with two symmetrical apical O atoms per Cu site, highlighted by the elongated octahedron in Fig. 1a. The Cu–O sheets are very distant from each other, resulting in a very weak inter-planar magnetic coupling. In contrast, in NBCO the two CuO_2 planes per unit cell are only 3.2 Å apart, and only one apical O per in-plane Cu contributes to the pyramid depicted in Fig. 1b. In CCO the absence of apical ligands allows the infinite, compact stacking of CuO_2 layers, with similar separation as in NBCO (Fig. 1c). The colour maps of Fig. 1d–f show important differences, beyond the overall similar dispersion shape, intensity and energy scale. Near the point $(0, 0)$ in the two-dimensional (2D)

reciprocal space, spin-wave excitations have vanishing energy and intensity in Bi2201, while they have nonzero energy and intensity in NBCO and CCO. In NBCO this corresponds to the gapped branch at $(1/2,1/2)$ seen in YBCO with INS (refs 22,23) and is due to the antiferromagnetic coupling between the adjacent CuO_2 planes. The other branch, expected to go to zero at $(0, 0)$, is not visible because its intensity vanishes while approaching the zone centre. The nonzero spin-wave energy of CCO near $(0, 0)$ is due to the interlayer magnetic coupling as well. In addition, the infinite-layer structure gives rise to a long-range out-of-plane spin correlation, as demonstrated below. For all samples the dispersion along the $(1/4, 1/4) \rightarrow (1/2, 0)$ line is larger than previously found in La_2CuO_4 (LCO), $Sr_2CuO_2Cl_2$ (SCOC) and Bi2212; and in CCO it is almost double than that in NBCO and Bi2201. In $(1/2, 0)$ the width of the magnon peak is clearly larger than in $(1/4, 1/4)$, well beyond the instrumental resolution (see Fig. 1g to i). This common feature was observed earlier in several square-lattice AF systems[8,16,24] and discussed in terms of possible coupling to higher-energy $\Delta S = 1/2$ 'spinon' excitations[25]. Whether the cross-section for such higher-energy excitations is stronger in RIXS than in INS, thus leading to systematic differences around $(1/2, 0)$ between the two techniques, is still unclear and will have to be further investigated[8].

The raw spectra shown in Fig. 2 were decomposed into a resolution-limited elastic peak, a resolution-limited phonon excitation, a weak resolution-limited bi-phonon excitation[26], an intense single-magnon peak and the bi-magnon tail (details in
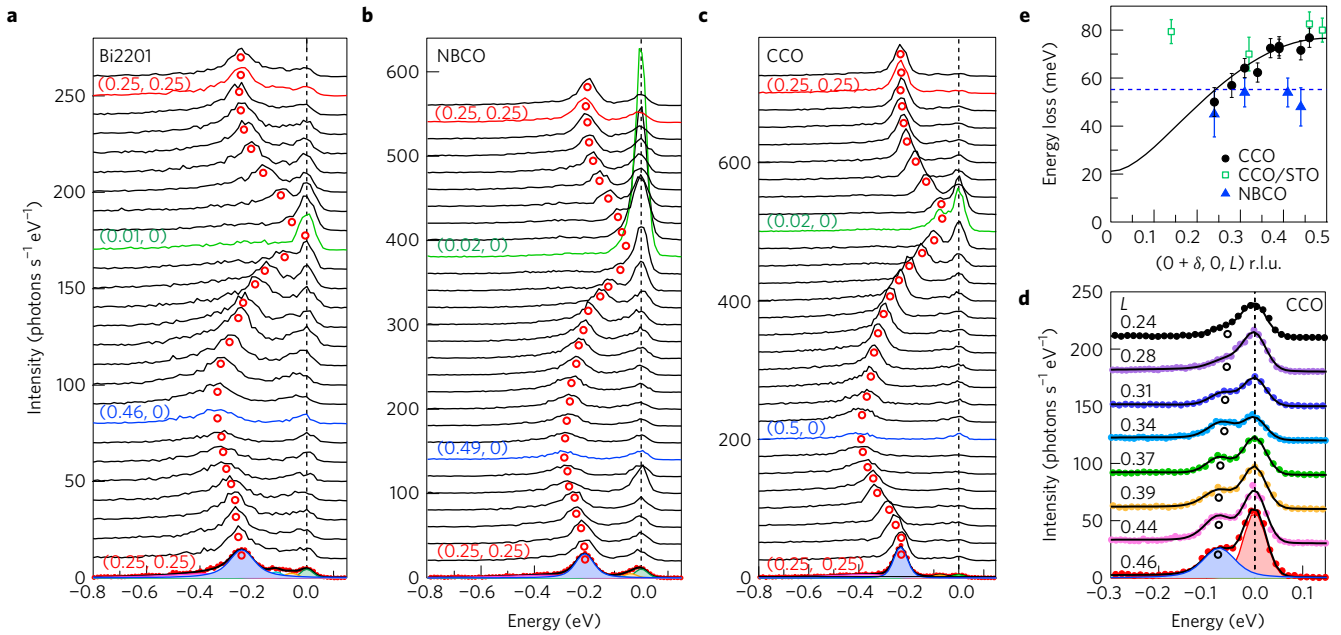
Figure 2 | Spectral fitting and three-dimensional dispersions of magnetic excitations in layered cuprates. a–c, The raw RIXS spectra for Bi2201 (**a**), NBCO (**b**) and CCO (**c**) measured at equally spaced positions along in-plane high-symmetry directions described in the inset of Fig. 1f. Each spectrum is shifted vertically for clarity. Examples of the five (three) peaks decomposition described in Supplementary Text and Supplementary Fig. 3 (Supplementary Fig. 5) are shown in the bottom spectra. Circles denote the peak positions of spin excitations determined by fitting. **d**, In CCO, dispersion of the peak at the zone centre along the normal direction of the CuO$_2$ planes: (0.015,0, L) trajectory for $L = 0.24$–0.46. **e**, Summary of the (δ, 0, L) dispersions of magnetic excitations for CCO ($\delta = 0.015$), superlattice CCO/STO ($\delta = 0.05$) and NBCO ($\delta = 0.02$). The L values are reduced to symmetry-equivalent reciprocal-space points within the 0–0.5 interval. The black line (blue dashed line) is the dispersion calculated with a $J_\perp = 4.3$ meV (6.2 meV) for CCO (NBCO). The error bars reflect the accuracy of the fitting procedure as detailed in Supplementary Information.

Supplementary Information). Besides the large dependence on the in-plane wavevector for all samples, the magnetic peak of CCO disperses also normally to the planes, along (0.015, 0, L) (Fig. 2d), constructing a three-dimensional (3D) exchange-bond network. To understand the long-range out-of-plane spin correlation we have grown and measured a (CaCuO$_2$)$_{3uc}$/(SrTiO$_3$)$_{2uc}$ superlattice where the AF structure is made inherently 2D by the intercalation of SrTiO$_3$ (STO) sheets to form a sort of artificial tri-layer cuprate. Consequently, the zone-centre gap is L-independent in (CCO)$_{3uc}$/(STO)$_{2uc}$ superlattice, as in NBCO but at variance from pure CCO (Fig. 2e). Interestingly, although the in-plane dispersion is the same in CCO and the CCO/STO superlattice (Supplementary Fig. 7), superconductivity has been realized in the CCO/STO superlattice[21,27], but not in the perfect infinite layer[28].

The magnon peak energy dispersions of our samples are presented in Fig. 3a–d together with that of LCO measured by INS (ref. 16). The experimental points are fitted with three models of increasing complexity and exchange integral spatial extent. Following ref. 29 we initially fitted all magnon dispersions with a simple nearest-neighbour Heisenberg model based on one effective in-plane exchange $J_\parallel$ parameter and two interlayer couplings $J_{\perp 1}$ and $J_{\perp 2}$, neglecting the magnetic anisotropy (Fig. 3e). The values of $J_\parallel$ are shown in Fig. 3h and do not follow an obvious trend versus the number of apical oxygens. The model correctly accounts for the L-dependence (independence) of the spin gap and gives $E\left(0, 0, (1/2)\right) \simeq 2\sqrt{2J_\parallel J_\perp}$ ($2\sqrt{J_\parallel J_\perp}$) in CCO (NBCO), where $J_\perp = J_{\perp 1} = J_{\perp 2}$ for CCO, $J_\perp = J_{\perp 1}$ for NBCO and neglecting the bilayer coupling $J_{\perp 2}$. Namely we find $J_\perp$ ($J_\perp$) = 158 meV (4.3 meV) for CCO and 123 meV (6.2 meV) for NBCO, which is comparable to 125 ± 5 meV (11 ± 2 meV) found for YBCO with INS (refs 22,23).

Although the simple nearest-neighbour Heisenberg model provides reasonable estimations of $J_\parallel$ and $J_\perp$, the large experimental dispersion along the MBZB calls for a better description of the in-plane magnetic interactions. Therefore, we fitted our experimental

results with the one-band Hubbard model with nearest-neighbour hopping t as in ref. 7, but keeping the same definition of $J_\perp$ for NBCO and CCO. We replaced $J_\parallel$ by three in-plane magnetic interactions up to second-nearest neighbours that are ultimately expressed by only two independent parameters, J and J_c (or t and U) (Fig. 3f). There, $J = 4(t^2/U) - 24(t^4/U^3)$ is the nearest-neighbour Cu–O–Cu superexchange integral, and $J_c = 80(t^4/U^3)$ is the so-called 'ring exchange' involving the four atoms of a plaquette. It can be shown that the maximum of magnon energy

$$E_{\max} = E\left(\frac{1}{2}, 0, L\right) = 2Z_c\left(J - \frac{J_c}{10}\right) \tag{1}$$

is mainly set by J, whereas J_c determines the energy dispersions along the zone boundary,

$$\Delta E_{\mathrm{MBZB}} = E\left(\frac{1}{2}, 0, L\right) - E\left(\frac{1}{4}, \frac{1}{4}, L\right) = \frac{3}{5}Z_cJ_c \tag{2}$$

where $Z_c = 1.18$ is a renormalization factor accounting for quantum fluctuations[30]. The fitting values are listed in Table 1 and summarized in Fig. 3i, together with the trend lines following equations (1) and (2). The fitting curves (dashed lines in Fig. 3a–d) are very satisfactory overall. However, the corresponding Hubbard model parameters imply $U < 6t$ for all samples, except LCO: as a consequence U is much smaller than that obtained from ARPES (ref. 31 and references therein), and the large-U hypothesis at the basis of the Hubbard model is not fulfilled.

This inadequacy of the one-band Hubbard model with only nearest-neighbour hopping in accounting for the details of magnon dispersion in cuprates is a longstanding issue that has led to the extension of the model with the second-nearest-neighbour direct hopping parameters t' and t'' (refs 32,33). Preferring a more phenomenological approach, we have simply relaxed the fitting
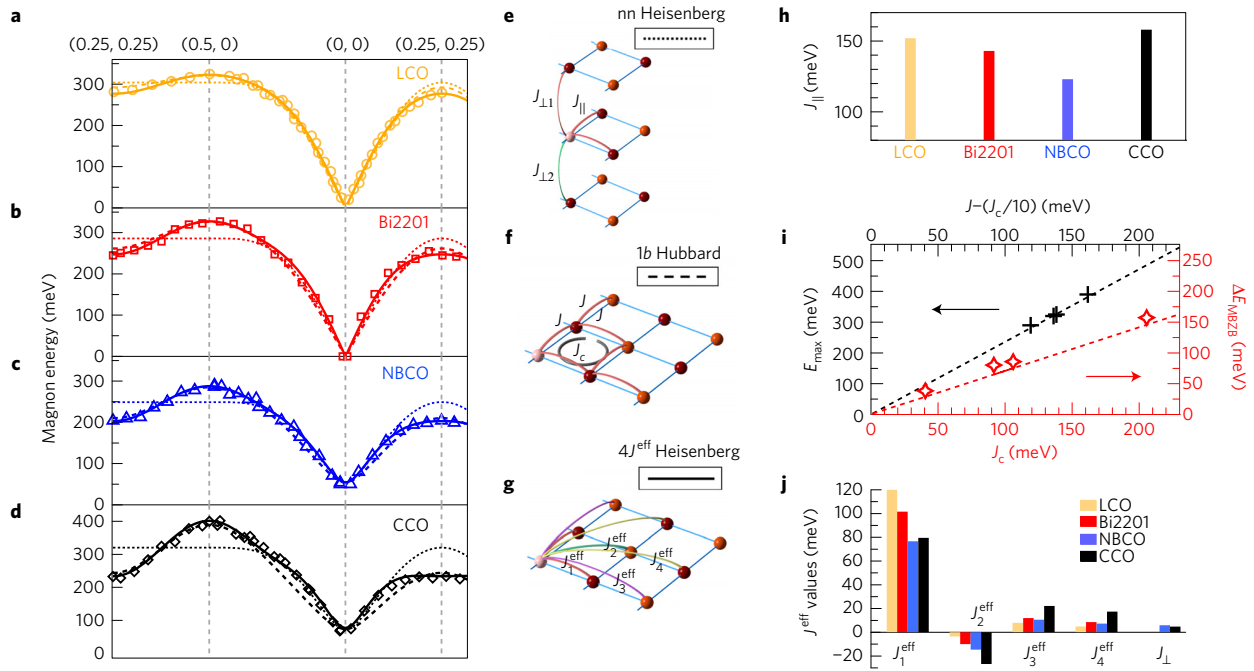
Figure 3 | Dispersion of the spin excitations and comparison to model calculations. a–d, Experimental magnon dispersion along the high-symmetry direction in antiferromagnetic Bi2201, NBCO, CCO (RIXS) and LCO (INS) (ref. 16), as indicated, fitted using the nearest-neighbour Heisenberg (nnH) model (dotted line), the one-band Hubbard (1bH) model (dashed line) and the phenomenological linear spin-wave Heisenberg model with four nearest-neighbour coupling parameters ($4J^{eff}$) (thick line). The error bars are smaller than symbol dimensions. **e–g,** Schematics of the nnH, 1bH and $4J^{eff}$ Heisenberg models, respectively. **h,** The $J_{\parallel}$ values determined from the nnH model. **i,** Linear dependence of $E_{max} = E(1/2, 0)$ (left/top axis, black symbols) and of ΔE_{MBZB} (right/bottom axis, red symbols) versus the one-band Hubbard model parameters J and J_c as defined in **f**; the lines follow equations (1,2) of the text. **j,** Effective parameters of the phenomenological spin-wave model based on four in-plane J^{eff} parameters as defined in **g**, and $J_{\perp}$ for NBCO and CCO.

Table 1 | The one-band Hubbard model parameters resulting from the least-squares fitting of the Bi2201, NBCO and CCO (present work) and LCO (ref. 16) spin-wave dispersion experimental data and leading to the dashed curves in Fig. 3a–d.

	n	z_{Cu-O}	E_{max}	ΔE_{MBZB}	J	J_c	$J_{\perp}$	U/t
LCO	2	2.42	325	38	140	41	–	8.7
Bi2201	2	2.58	326	80	148	92	–	6.2
NBCO	1	2.38	289	86	130	106	7	5.5
CCO	0	–	400	157	182	206	6	4.9

n and z_{Cu-O} are the number of apical oxygens and their distance in Å, respectively. The other parameters E_{max}, ΔE_{MBZB} and J are expressed in meV. A more complete parameter set is listed in Supplementary Table 2.

constraints, abandoning the Hubbard model and adding longer-range effective exchange terms up to fourth-nearest neighbours[34], as illustrated in Fig. 3g; we have also tested longer-range parameters, up to sixth-nearest neighbours and found that fittings improve only marginally (Supplementary Fig. 9). Therefore, we base our analysis on the $4J^{eff}$ model fitting. The resulting dispersion is given in Fig. 3a–d by the solid lines, which are considerably closer to the experimental points than the dashed ones: the fitting improves particularly at the intermediate $q_{\parallel}$ values, and the residual error is 2 to 3 times smaller. The $4J^{eff}$ parameters are listed in Supplementary Table 3 and plotted in Fig. 3j. The main result is that the negative (ferromagnetic) exchange across the diagonal of the plaquette (J_2^{eff}), and the positive (antiferromagnetic) coupling with next-nearest neighbour along the edge (J_3^{eff}) both grow from LCO to Bi2201, to NBCO, to CCO, indicating an increasing importance of longer-range interactions. We note that J_2^{eff} is consistently negative, providing a ferromagnetic coupling along the diagonal that acts to stabilize the antiferromagnetic structure. In contrast, J_3^{eff} is positive, introducing frustration along the Cu–O–Cu direction, where the second-neighbour moments are parallel despite their antiferromagnetic coupling.

In summary, the fittings with the two models going beyond nearest-neighbour interaction have shown that 'less' apical oxygens imply larger zone boundary dispersion ΔE_{MBZB}, and larger dispersion requires larger long-range exchange parameters (J_c, or J_2^{eff}, J_3^{eff}); conversely we confirm that E_{max}, the maximum energy at (1/2,0), and the related nearest-neighbour exchange parameters ($J_{\parallel}$, J, J_1^{eff}) are not univocally related to apical oxygens. To complete this phenomenological analysis we look also at the ligand field excitations, easily accessible by RIXS, and known to be strongly influenced by the local coordination of the Cu ion[35]. In particular, in the spectra of Fig. 4a we highlight the energy of the $3d_{z^2}$ orbital excitation (E_{z^2}) as obtained from the dd-excitation region of the RIXS spectra. The assignment of the $3d_{z^2}$ orbital excitation in CCO was unambiguously verified by referring to the spectra analysed in ref. 35 and with the *ab initio* quantum chemical calculations of ref. 36. The local coordination of CCO/STO consists of two CuO$_2$ planes with no apicals (the inner one and that facing the Ca^{2+} plane) and one plane with one apical oxygen belonging to the SrO layer (ref. 21). The dd excitations in CCO/STO are very similar to that of CCO due to the small average fraction of apical oxygen per Cu site (Fig. 4a). We find that E_{z^2} is positively correlated with ΔE_{MBZB}, as illustrated in the bottom panel of Fig. 4b. Here, closer apical oxygens are known to reduce the split-off energy of the $3d_{z^2}$ orbital and to increase its weight in the
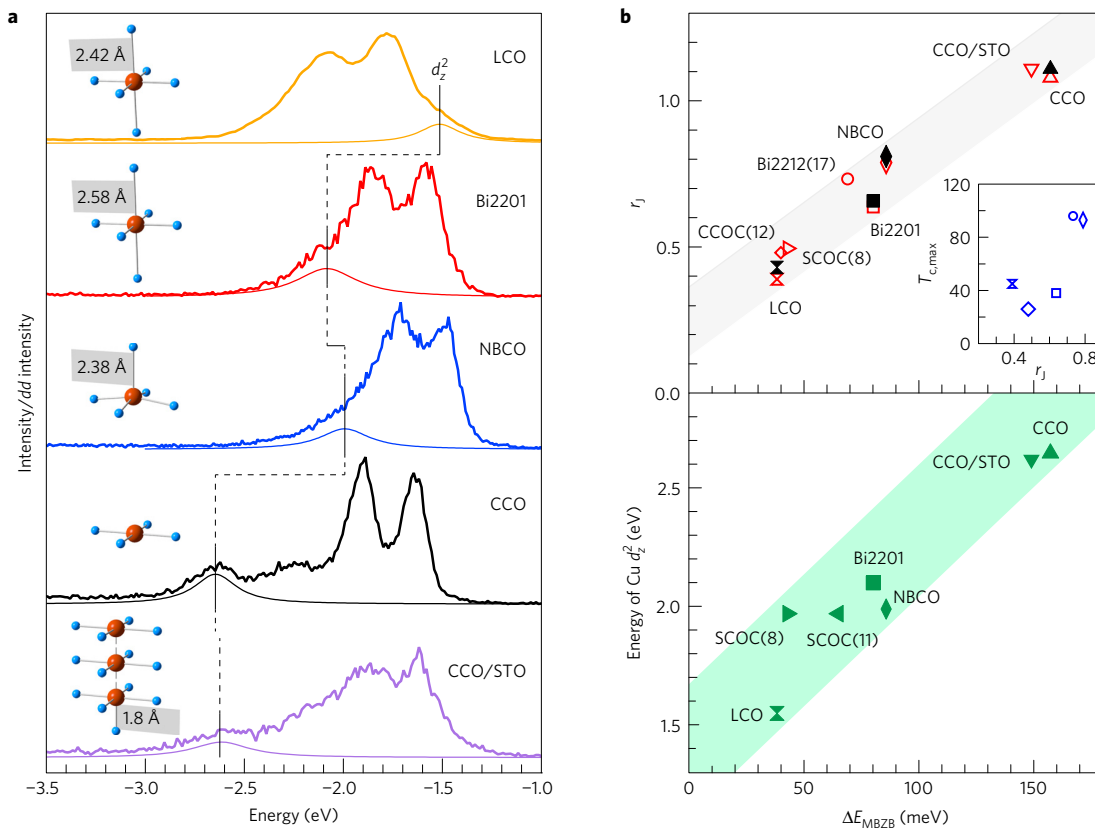
Figure 4 | Phenomenological relation of the spin-wave dispersions with ligand field d_{z^2} orbital excitations and exchange range parameter. a, Normalized RIXS spectra, measured at $\mathbf{q}_{\parallel} \sim (0.48, 0)$ with π-polarization, in the dd excitation region: the d_{z^2} orbital components are shown as thin lines. The local Cu–O coordination is sketched in the inset. For CCO/STO the distance between two nearby CuO$_2$ planes is not to scale due to space limitations. **b**, Correlation of the exchange range parameter (r_J) defined in the text (top) and the energy of Cu d_{z^2} (bottom) with ΔE_{MBZB}. Data of Sr$_2$CuO$_2$Cl$_2$ (SCOC) (refs 8,11), Ca$_2$CuO$_2$Cl$_2$ (CCOC) (ref. 12) and Bi$_2$Sr$_2$YCu$_2$O$_8$ (Bi2212) (ref. 17) are also included. The open red symbols are obtained from the 1b Hubbard model according to equations (1) and (2) and Supplementary Equation 29; the full black points are obtained from the $4J^{eff}$ Heisenberg model. The inset shows $T_{c,max}$ plotted against the range parameter r_J. The $T_{c,max}$ values follow ref. 6. The shadows highlight trends and are not intended to propose analytical relationships.

ground state[35]: it appears clearly that apical oxygens tend to localize charge in the $3d_{z^2}$ orbitals, thus producing an effective screening by the polarizable charge reservoir layer[37].

Then the crucial question arises: how much are apical oxygens influencing superconductivity in cuprates? Pavarini *et al.*[18] pointed out that the maximal T_c in each family of cuprates scales with the next-nearest-neighbour hopping, which grows with the distance of apical oxygen to the CuO$_2$ plane. The link between exchange parameters and hopping integrals is not straightforward, and more sophisticated theoretical work is needed to map the effective J values into multi-band and multi-hopping parameters. However, inspired by the hopping range parameter $r \sim (t'/t)(r \sim (|t'| + |t''|/|t|))$ discussed in ref. 18 (ref. 38), and considering that J_1^{eff}, J_2^{eff} and J_3^{eff} are related to t^2, $(t')^2$ and $(t'')^2$, respectively[33], we define $r_J = \left(\sqrt{|J_2^{eff}|} + \sqrt{J_3^{eff}} \right) / \sqrt{J_1^{eff}}$. In Fig. 4b we show that r_J increases with ΔE_{MBZB}, therefore validating its definition as 'exchange range parameter'. In the inset we plot $T_{c,max}$ versus r_J, showing a trend reminiscent of the relation between $T_{c,max}$ and the hopping range parameter in ref. 18. This trend suggests a positive correlation that shall be confirmed through systematic RIXS investigations of other cuprate families. Our results suggest looking directly into the role of longer-range exchange interactions, which may change the kinematics of the spin-fluctuation-mediated pairing interaction. However, this goes beyond the present work and has to be addressed in future calculations in the spirit of ref. 39.

Multi-orbital Hubbard model calculations[38,40,41] and our present work suggest that an ideal hole-doped cuprate superconductor

would maximize the long-range hopping and minimize the $3d_{z^2}$ character of the Fermi surface. These properties are favoured by structures with less and farther apical oxygens (larger crystal field splitting), which are determined also by the Madelung potential difference between in-plane and apical oxygens[40,42], a difference traceable back to the details of the charge reservoir structure and chemical composition. Unfortunately, infinite-layer compounds, such as CCO and (SrCa)CuO$_2$, include apical oxygens whenever hole-doped (and superconducting). Other factors are surely influencing $T_{c,max}$, such as buckling or defects, and they might explain why $T_{c,max} \sim 110$ K was found in (Sr,Ca)CuO$_2$ with the doping introduced by planar defects[43,44] but only $T_{c,max} \sim 50$ K in CCO/STO superlattices with doping introduced by oxygen intercalation at CCO–STO interfaces[27,45]. Tri-layer compounds such as Bi2223 and Tl2223 indeed reach very high T_c, because the inner CuO$_2$ layer has no apical, but its effective doping is also lower than nominal[46]. This could explain why tri-layer cuprates usually have the largest $T_{c,max}$, as they provide an ideal trade-off between long-range in-plane hopping and efficient interlayer charge transfer.

Methods

Methods, including statements of data availability and any associated accession codes and references, are available in the online version of this paper.

References

1. Ogata, M. & Fukuyama, H. The t-J model for the oxide high-T_c superconductors. *Rep. Prog. Phys.* **71,** 036501 (2008).
2. Scalapino, D. J. A common thread: the pairing interaction for unconventional superconductors. *Rev. Mod. Phys.* **84,** 1383–1417 (2012).
3. Mallett, B. P. P. *et al.* Dielectric versus magnetic pairing mechanisms in high-temperature cuprate superconductors investigated using Raman scattering. *Phys. Rev. Lett.* **111,** 237001 (2013).
4. Munoz, D., Illas, F., Moreira, I. & de, P. R. Accurate prediction of large antiferromagnetic interactions in high-T_c HgBa$_2$Ca$_{n-1}$Cu$_n$O$_{2n+2+\delta}$ ($n=2, 3$) superconductor parent compounds. *Phys. Rev. Lett.* **84,** 1579–1582 (2000).
5. Ellis, D. S. *et al.* Correlation of the superconducting critical temperature with spin and orbital excitation energies in (Ca$_x$La$_{1-x}$)(Ba$_{1.75-x}$La$_{0.25+x}$)Cu$_3$O$_y$ as measured by resonant inelastic X-ray scattering. *Phys. Rev. B* **92,** 104507 (2015).
6. Eisaki, H. *et al.* Effect of chemical inhomogeneity in bismuth-based copper oxide superconductors. *Phys. Rev. B* **69,** 064512 (2004).
7. Coldea, R. *et al.* Spin waves and electronic interactions in La$_2$CuO$_4$. *Phys. Rev. Lett.* **86,** 5377–5380 (2001).
8. Plumb, K. W., Savici, A. T., Granroth, G. E., Chou, F. C. & Kim, Y.-J. High-energy continuum of magnetic excitations in the two-dimensional quantum antiferromagnet Sr$_2$CuO$_2$Cl$_2$. *Phys. Rev. B* **89,** 180410(R) (2014).
9. Braicovich, L. *et al.* Magnetic excitations and phase separation in the underdoped La$_{2-x}$Sr$_x$CuO$_4$ superconductor measured by resonant inelastic X-ray scattering. *Phys. Rev. Lett.* **104,** 077002 (2010).
10. Ament, L. J. P., Ghiringhelli, G., Moretti Sala, M., Braicovich, L. & van den Brink, J. Theoretical demonstration of how the dispersion of magnetic excitations in cuprate compounds can be determined using resonant inelastic X-ray scattering. *Phys. Rev. Lett.* **103,** 117003 (2009).
11. Guarise, M. *et al.* Measurement of magnetic excitations in the two-dimensional antiferromagnetic Sr$_2$CuO$_2$Cl$_2$ insulator using resonant X-ray scattering: evidence for extended interactions. *Phys. Rev. Lett.* **105,** 157006 (2010).
12. Lebert, B. W. *et al.* Resonant inelastic X-ray scattering study of spin-wave excitations in the cuprate parent compound Ca$_2$CuO$_2$Cl$_2$. *Phys. Rev. B* **95,** 155110 (2017).
13. Le Tacon, M. *et al.* Intense paramagnon excitations in a large family of high-temperature superconductors. *Nat. Phys.* **7,** 725–730 (2011).
14. Dean, M. P. M. *et al.* Persistence of magnetic excitations in La$_{2-x}$Sr$_x$CuO$_4$ from the undoped insulator to the heavily overdoped non-superconducting metal. *Nat. Mater.* **12,** 1019–1023 (2013).
15. Minola, M. *et al.* Collective nature of spin excitations in superconducting cuprates probed by resonant inelastic X-Ray scattering. *Phys. Rev. Lett.* **114,** 217003 (2016).
16. Headings, N. S., Hayden, S. M., Coldea, R. & Perring, T. G. Anomalous high-energy spin excitations in the high-T_c superconductor-parent antiferromagnet La$_2$CuO$_4$. *Phys. Rev. Lett.* **105,** 247001 (2010).
17. Dalla Piazza, B. *et al.* Unified one-band Hubbard model for magnetic and electronic spectra of the parent compounds of cuprate superconductors. *Phys. Rev. B* **85,** 100508(R) (2012).
18. Pavarini, E., Dasgupta, I., Saha-Dasgupta, T., Jepsen, O. & Andersen, O. K. Band-structure trend in hole-doped cuprates and correlation with $T_{c,max}$. *Phys. Rev. Lett.* **87,** 047003 (2001).
19. Peng, Y. Y. *et al.* Disappearance of nodal gap across the insulator-superconductor transition in a copper-oxide superconductor. *Nat. Commun.* **4,** 2459 (2013).
20. Salluzzo, M. *et al.* Thickness effect on the structure and superconductivity of Nd$_{1.2}$Ba$_{1.8}$Cu$_3$O$_z$ epitaxial films. *Phys. Rev. B* **72,** 134521 (2005).
21. Di Castro, D. *et al.* Occurrence of a high-temperature superconducting phase in (CaCuO$_2$)$_n$/(SrTiO$_3$)$_m$ superlattices. *Phys. Rev. B* **86,** 134524 (2012).
22. Reznik, D. *et al.* Direct observation of optical magnons in YBa$_2$Cu$_3$O$_{6.2}$. *Phys. Rev. B* **53,** R14741 (1996).
23. Hayden, S. M., Aeppli, G., Perring, T. G., Mook, H. A. & Doğan, F. High-frequency spin waves in YBa$_2$Cu$_3$O$_{6.15}$. *Phys. Rev. B* **54,** R6905 (1996).
24. Dalla Piazza, B. *et al.* Fractional excitations in the square-lattice quantum antiferromagnet. *Nat. Phys.* **11,** 62–68 (2014).
25. Ho, C. M., Muthukumar, V. N., Ogata, M. & Anderson, P. W. Nature of spin excitations in two-dimensional Mott insulators: undoped cuprates and other materials. *Phys. Rev. Lett.* **86,** 1626–1629 (2001).
26. Ament, L. J. P., Van Veenendaal, M. & Van Den Brink, J. Determining the electron–phonon coupling strength from resonant inelastic X-ray scattering at transition metal L-edges. *Europhys. Lett.* **95,** 27008 (2011).
27. Di Castro, D. *et al.* High-T_c superconductivity at the interface between the CaCuO$_2$ and SrTiO$_3$ insulating oxides. *Phys. Rev. Lett.* **115,** 147001 (2015).
28. Adachi, S., Yamauchi, H., Tanaka, S. & Môri, N. High-pressure synthesis of superconducting Sr–Ca–Cu–O samples. *Physica C* **208,** 226–230 (1993).
29. Tranquada, J. M., Shirane, G., Keimer, B., Shamoto, S. & Sato, M. Neutron scattering study of magnetic excitations in YBa$_2$Cu$_3$O$_{6+x}$. *Phys. Rev. B* **40,** 4503–4516 (1989).
30. Singh, R. R. P. Thermodynamic parameters of the $T=0$, spin $=1/2$ square-lattice Heisenberg antiferromagnet. *Phys. Rev. B* **39,** 9760–9763 (1989).
31. Tohyama, T. & Maekawa, S. Angle-resolved photoemission in high T_c cuprates from theoretical viewpoints. *Supercond. Sci. Technol.* **13,** R17 (2000).
32. MacDonald, A. H., Girvin, S. M. & Yoshioka, D. t/U expansion for the Hubbard model. *Phys. Rev. B* **37,** 9753–9756 (1988).
33. Delannoy, J. Y., Gingras, M. J. P., Holdsworth, P. C. W. & Tremblay, A. M. Low-energy theory of the t-t'-t''-U Hubbard model at half-filling: interaction strengths in cuprate superconductors and an effective spin-only description of La$_2$CuO$_4$. *Phys. Rev. B* **79,** 235130 (2009).
34. Toth, S. & Lake, B. Linear spin wave theory for single-Q incommensurate magnetic structures. *J. Phys. Condens. Matter* **27,** 166002 (2015).
35. Sala, M. M. *et al.* Energy and symmetry of dd excitations in undoped layered cuprates measured by Cu L$_3$ resonant inelastic X-ray scattering. *New J. Phys.* **13,** 043026 (2011).
36. Hozoi, L., Siurakshina, L., Fulde, P. & van den Brink, J. *Ab initio* determination of Cu 3d orbital energies in layered copper oxides. *Sci. Rep.* **1,** 65 (2011).
37. Johnston, S. *et al.* Systematic study of electron–phonon coupling to oxygen modes across the cuprates. *Phys. Rev. B* **82,** 064513 (2010).
38. Sakakibara, H. *et al.* Orbital mixture effect on the Fermi-surface-T_c correlation in the cuprate superconductors: bilayer vs. single layer. *Phys. Rev. B* **89,** 224505 (2014).
39. Dahm, T. *et al.* Strength of the spin-fluctuation-mediated pairing interaction in a high-temperature superconductor. *Nat. Phys.* **5,** 217–221 (2009).
40. Sakakibara, H., Usui, H., Kuroki, K., Arita, R. & Aoki, H. Two-orbital model explains the higher transition temperature of the single-layer Hg-cuprate superconductor compared to that of the La-cuprate superconductor. *Phys. Rev. Lett.* **105,** 057003 (2010).
41. Sakakibara, H., Usui, H., Kuroki, K., Arita, R. & Aoki, H. Origin of the material dependence of T_c in the single-layered cuprates. *Phys. Rev. B* **85,** 064501 (2012).
42. Ohta, Y., Tohyama, T. & Maekawa, S. Apex oxygen and critical temperature in copper oxide superconductors: universal correlation with the stability of local singlets. *Phys. Rev. B* **43,** 2968–2982 (1991).
43. Azuma, M., Hiroi, Z., Takano, M., Bando, Y. & Takeda, Y. Superconductivity at 110 K in the infinite-layer compound (Sr$_{1-x}$Ca$_x$)$_{1-y}$CuO$_2$. *Nature* **356,** 775–776 (1992).
44. Zhang, H. *et al.* Identity of planar defects in the 'Infinite-layer' copper oxide superconductor. *Nature* **370,** 352–354 (1994).
45. Di Castro, D. *et al.* T_c up to 50 K in superlattices of insulating oxides. *Supercond. Sci. Technol.* **27,** 044016 (2014).
46. Ideta, S. I. *et al.* Energy scale directly related to superconductivity in high-T_c cuprates: universality from the temperature-dependent angle-resolved photoemission of Bi$_2$Sr$_2$Ca$_2$Cu$_3$O$_{10+\delta}$. *Phys. Rev. B* **85,** 104515 (2012).

Author contributions

G.G., Y.Y.P. and L.B. conceived and designed the experiments with suggestions from B.K.; G.G., Y.Y.P., L.B., M.M., G.D., N.B.B., K.K., A.A., M.C., M.L.T., D.D.C. and G.M.D.L. performed the measurements. D.D.C. and G.B. grew and characterized the CCO and CCO/STO thin films; M.S. and G.M.D.L. grew and characterized the NBCO thin films; Y.Y.P., X.S. and X.J.Z. synthesized, grew and characterized the Bi2201 single crystals. Y.Y.P. and G.G. analysed the experimental data; G.G., Y.Y.P., M.C. and M.M. performed the model calculations. Y.Y.P. and G.G. wrote the manuscript with the help of M.L.T., B.K. and M.M., and contributions from all authors.

Additional information

Supplementary information is available in the online version of the paper. Reprints and permissions information is available online at www.nature.com/reprints. Publisher's note: Springer Nature remains neutral with regard to jurisdictional claims in published maps and institutional affiliations. Correspondence and requests for materials should be addressed to G.G.

Competing financial interests

The authors declare no competing financial interests.

Methods

Sample preparation. Single crystals of $Bi_2Sr_{0.9}La_{1.1}CuO_{6+\delta}$ (Bi2201, $p = 0.03$) were grown by the travelling solvent floating zone method. The sample growth and characterization methods have been reported previously[19]. The samples were cleaved out of vacuum to expose a fresh surface. $Nd_{1.2}Ba_{1.8}Cu_3O_6$ (NBCO) films were deposited by high-oxygen-pressure diode sputtering on $SrTiO_3$ (100) single crystals. After deposition, the undoped NBCO film was obtained by annealing the as-grown $Nd_{1.2}Ba_{1.8}Cu_3O_7$ films in an argon atmosphere (10 mbar) for 48 h (ref. 20). The $CaCuO_2$ films and $CaCuO_2/SrTiO_3$ superlattice were grown by pulsed laser deposition (KrF excimer laser, $\lambda = 248$ nm) on 5×5 mm^2 $NdGaO_3$ (110) substrates[21,27]. Two targets, with $CaCuO_2$ and $SrTiO_3$ nominal composition, mounted on a multitarget system, were used. The STO target is a commercial crystal obtained from Crystal, GmbH. The CCO target was prepared by standard solid state reaction, according to the following procedure: stoichiometric mixtures of high-purity $CaCO_3$ and CuO powders were calcined at 860 °C in air for 24 h, pressed to form a disk, and finally heated at 900 °C for 12 h. The substrate was placed at about 3 cm from the targets on a heated holder and its temperature during the deposition of the films was $T \simeq 600$ °C. The deposition chamber was first evacuated down to $P \simeq 10^{-5}$ mbar and then oxygen atmosphere at a pressure of about 5×10^{-2} mbar was used for the growth. At this pressure, both CCO films and CCO/STO superlattice are insulating. At the end of the deposition, the films were cooled down at the growth pressure. The CCO films thickness is about 100 unit cells (~320 Å). The superlattice CCO/STO is formed by 20 repetitions of the 'supercell' CCO_3/STO_2, made by 3 unit cells of CCO and 2 unit cells of STO. Reciprocal lattice units (r.l.u.) were defined using the lattice constants $a = b = 3.86$ Å and $c = 24.4$ Å for Bi2201, $a = b = 3.84$ Å and $c = 11.7$ Å for NBCO, $a = b = 3.85$ Å and $c = 3.2$ Å (17.6 Å) for CCO (superlattice CCO/STO).

RIXS measurements. The RIXS measurements were performed at the new beam line ID32 of ESRF (The European Synchrotron, Grenoble, France) using the new high-resolution ERIXS spectrometer. ERIXS allows, for the first time in the soft X-ray range, experiments with complete sample orientation control and the possibility of changing in a continuous way the scattering angle of 2θ (50° to 150°),

as shown in Supplementary Fig. 1a. The resonant conditions were achieved by tuning the energy of the incident X rays to the maximum of the Cu L_3 absorption peak, around 931 eV. The total instrumental bandwidth (BW) of 55 meV at 931 eV (resolving power = 17,000) has been obtained with a 30 (15) μm entrance (exit) slit on the monochromator, a 4 μm spot size on the sample, an 800 lines mm^{-1} grating of the monochromator, a 1,400 lines mm^{-1} grating of the spectrometer, and the single photon detection mode in the Princeton 2048×2048 13.5 μm pixel detector, cooled at -110 °C by liquid nitrogen. The samples were cooled at 35 K, and were mounted on the 6-axis in-vacuum Huber diffractometer/manipulator. The instrumental BW was measured as the full-width at half-maximum of the non-resonant diffuse scattering from polycrystalline graphite (carbon tape). The typical size of the Brillouin zone in cuprates is 0.81 Å^{-1} (0.5 r.l.u.) and the maximum total momentum transfer is 0.91 Å^{-1} ($2\theta = 150°$), which allows one to cover the whole first Brillouin zone along the [100] or [010] direction (Supplementary Fig. 1b). In the specular geometry, by changing the scattering angle 2θ one can measure the [001] direction at the Brillouin zone centre (Supplementary Fig. 1b). In-plane dispersion was measured with fixed $2\theta = 149°$. The exact position of the elastic (zero energy loss) line was determined by measuring, for each transferred momentum, a non-resonant spectrum of silver paint or carbon tape. All data were obtained with π incident polarization (parallel to the scattering plane) to maximize the single-magnon signal[10,47]. Each spectrum is the result of 15 or 20 min total accumulation (sum of individual spectra of 30 s).

Data availability. The data that support the plots within this Article and other findings of this study are available from the corresponding author upon reasonable request. For convenience, the spin excitation energy dispersions for Bi2201, NBCO and CCO, as obtained from RIXS spectra, are explicitly reported in Supplementary Table 5.

References

47. Braicovich, L. *et al*. Momentum and polarization dependence of single-magnon spectral weight for Cu L3-edge resonant inelastic X-ray scattering from layered cuprates. *Phys. Rev. B* **81,** 174533 (2010).